# Neutron production in coincidence with fragments from the $^{40}$Ca + H reaction at $E_{lab}=357A$ and $565A$ MeV

C. Tuvè,[1] S. Albergo,[1] D. Boemi,[1] Z. Caccia,[1] C.-X. Chen,[3] S. Costa,[1] H. J. Crawford,[4] M. Cronqvist,[2] J. Engelage,[4] L. Greiner,[4] T. G. Guzik,[3] C. N. Knott,[5] A. Insolia,[1] P. J. Lindstrom,[2] J. W. Mitchell,[8] R. Potenza,[1] G. V. Russo,[1] A. Soutoul,[7] O. Testard,[7] A. Tricomi,[1] C. E. Tull,[3] C. J. Waddington,[5] W. R. Webber,[6] and J. P. Wefel[3]

(TRANSPORT Collaboration)

[1]*University of Catania and INFN, I-95129 Catania, Italy*
[2]*Lawrence Berkeley National Laboratory, Berkeley, California 94720*
[3]*Louisiana State University, Baton Rouge, Louisiana 70803*
[4]*Space Science Laboratory, University of California, Berkeley, California 94720*
[5]*University of Minnesota, Minneapolis, Minnesota 55455*
[6]*University of New Mexico, Las Cruces, New Mexico 88003*
[7]*Service d'Astrophysique, C.E.N. Saclay, France 91191*
[8]*NASA/Goddard Space Flight Center, Greenbelt, Maryland 20771*

(Received 31 July 1998)

Neutron production, in coincidence with fragments emitted in the $^{40}$Ca+H reaction at $E_{lab}=357A$ and 565*A* MeV, has been measured using a 3-module version of the multifunctional neutron spectrometer MUFFINS. The mean neutron multiplicities for neutrons detected in the angular range covered by MUFFINS ($0°-3.2°$) have been estimated from the comparison between the neutron cross sections, in coincidence with the fragments, and the elemental cross sections. We have found evidence for a preequilibrium emission of prompt neutrons in superposition to a ''slower'' deexcitation of the equilibrated remnant by emission of nucleons and fragments, as already seen in inclusive rapidity distributions. The energy dependence of the inclusive neutron production cross sections, measured in a previous work, is here interpreted as due to the stronger neutron focusing in the forward direction at the higher energy. Comparison with a BNV+phase space coalescence model is discussed. [S0556-2813(99)01101-2]

PACS number(s): 25.75.−q, 29.40.Mc

## I. INTRODUCTION

Fragmentation processes in nuclear collisions at intermediate energies are currently among the most widely studied topics both from an experimental and a theoretical point of view. They are not only essential tools for studies of the nuclear equation of state (EOS) [1–5] but are also of great interest in astrophysics [6,7].

Actually, fragment excitation functions for proton-nucleus interactions in the 1 to 20 GeV range suggested that fragmentation, in this energy range [8,9], is the result of a two-step process. The formation of the remnant occurs in a first step involving prompt particle emission while the breakup of the remnant (or its decay) occurs in a slower second step. In recent years, further progress has been made possible by exclusive studies of multifragmentation (MF) [10,11]. For example, the EOS Collaboration studied the MF of 1*A* GeV gold on carbon [11] and was able to show that following its formation in a prompt preequilibrium step, the remnant undergoes equilibration prior to its breakup. Thus, collisions between ''large'' and ''small'' nuclei seem very interesting, at least in this energy range.

The TRANSPORT Collaboration was formed to accomplish an accurate systematic measurement of the cross sections for the interaction of the heavy ions, expected to be found in primary galactic cosmic rays, with targets of the most abundant nuclei found in the interstellar medium, that is, H and He [12–15]. The aim of this systematic study is to build a sufficiently large database of cross sections to calibrate and refine the transport models that attempt to relate the primary composition of the cosmic rays at their galactic source to the modified composition observed on or near the Earth. In addition to the main motivations of the TRANSPORT Collaboration, the reaction mechanism in itself and the properties of the nuclear matter in nucleus-proton collisions are worth studying.

Finally, while charged particle emission has been extensively studied, neutron emission has received lesser attention, mainly due to the technical difficulties inherent to the detection of neutral particles [16–20], which on the other hand seems quite interesting just because of the insensitivity of neutrons to the Coulomb field. Therefore the neutron detection in nuclear collisions from intermediate to relativistic energies looks a very promising source of interesting physics.

We have studied the reaction $^{40}$Ca+H at 565*A* and 357*A* MeV. To detect neutrons and measure their energy spectra, angular distributions and multiplicities we designed and built a completely new-concept modular neutron spectrometer, called MUFFINS (multifunctional neutron spectrometer) [21,22].

We have published the energy spectra, angular and rapidity distributions, and total inclusive cross sections for neutrons emitted in the collision. Some interesting insights on the reaction mechanism have been obtained by looking at the rapidity distributions [23].

 

In this paper we will present, for the same reaction, the neutron cross sections measured in coincidence with the fragment production [13,15]. Section II presents some details of the experimental setup and data analysis. Sec. III deals with the neutron production cross sections and includes a discussion of the results. Conclusions are given in Section IV.

## II. EXPERIMENTAL SETUP AND ANALYSIS PROCEDURE

The experiment was performed at the Heavy Ion Spectrometer System (HISS) facility of the Lawrence Berkeley National Laboratory. A low intensity (less than 2000 ions/sec typically) $^{40}Ca^{20+}$ beam was accelerated by the Bevalac accelerator. Two different energies of the calcium ion beam were used, 600*A* and 400*A* MeV. The complete experimental setup is presented in Ref. [14] where all details can be found.

The experimental apparatus was divided into subsystems: the beam detection system, the liquid hydrogen target, the HISS magnet, the downstream section for charged particle detection (drift chamber and TOF wall), and the neutron detector. The beam detection system provided the experiment triggers, incoming particle vectors, beam counts, and charge states. The target system, where the interaction takes place, contained liquid hydrogen condensed directly into a target vessel. The target thickness was $0.254 \pm 0.004$ g/cm$^2$. The energies of the beam at the target were 565*A* and 357*A* MeV, respectively, due to significant energy loss in the upstream detectors.

The fragment charge was measured immediately after the interaction by two post-target measuring detectors. The first one was a solid state detector (SSD), the second one was a scintillator (BV). The HISS dipole magnet swept almost all charged fragments into the downstream section where the charged particle detectors were located. Again all details of the downstream systems can be found in Ref. [14].

The neutron detector MUFFINS was located on the incident beam line away from the charged particle detectors. MUFFINS is a modular detector made of several individual discs. For this measurement, it was comprised of three modules.

The MUFFINS modules are discs of NE102A plastic scintillator and are 1 m in diameter and 3 cm thick [21,22]. Each disc, in the present measurements, was instrumented with five HAMAMATSU R1398 PMT's, placed at the vertices of a regular pentagon around the disc edge. Each PMT was coupled to the disc through a short cylindrical perspex light pipe.

The MUFFINS discs were arranged in a coaxial cylindrical packet placed along the direction of the undeflected beam, at 0°, 9 m downstream of the target. In this position the discs covered a 3.2° angular range around the beam direction. This is a rather good geometrical acceptance, since at relatively high incident energies, in reverse kinematics reaction such as $^{40}Ca+H$, nuclear fragments as well as neutrons are likely to be emitted in a narrow cone about the direction of the incident beam. To determine the time of flight $\tau_0$ and position coordinates $(x,y)$ of each hit on the MUFFINS discs we adopted the technique described in Ref. [21] which uses equations written in multiple elliptical coordinate systems (MECS).

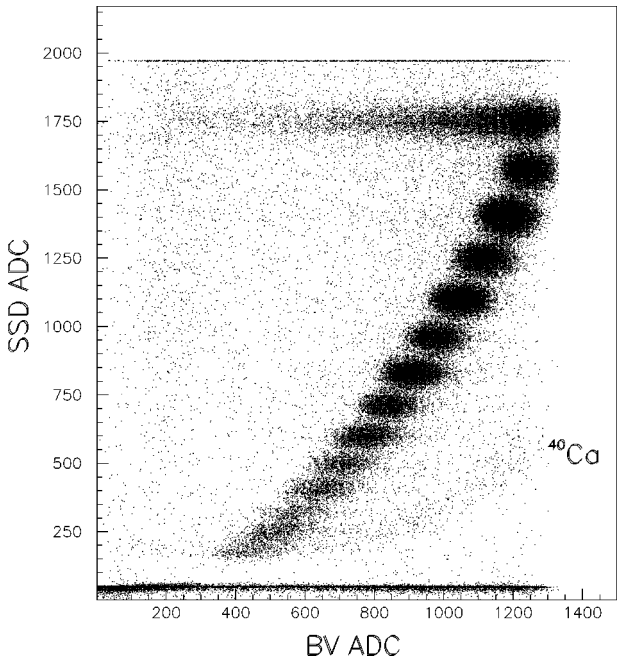


FIG. 1. A typical scatter plot SSD ADC vs BV ADC for $^{40}$Ca at 565*A* MeV.

Multiple hits in the MUFFINS discs are discarded by a cut on the position reconstruction error. Single hits are tagged *neutrons* if no hit occurred in the preceding disc. In fact, starting from the second disc, if a hit were due to a primary charged particle or to a secondary (neutral or charged) particle, it would have been observed in the preceding disc as well. The first disc is used as a veto for the primary charged particles. This will veto also neutrons simultaneously arriving onto the first disc of the detector, thus producing a lowering of the effective neutron detection efficiency. For the three-module version of MUFFINS the resulting lowering in the efficiency was of the order of 3%.

An absolute time of flight calibration was obtained by sending the Ca beam directly onto the discs. Further details about the MUFFINS detector, its calibration and data analysis procedures are discussed in Ref. [23].

For each run, data were collected both with and without liquid hydrogen in the vessel for a proper background subtraction in the neutron production cross section. The target correlated background (see, for example, the discussion in Ref. [24]) was not measured in this experiment. We have estimated its amount and found it negligible. Further details about thick target corrections and target correlated background, properly taken into account in the analysis procedure, are to be found in Ref. [23].

We selected neutrons using both triggers available in the experiment, that is ''interaction trigger'' [13,14], which removed most the uninteracted beam projectiles, and ''beam trigger'' [13,14], which accepted mainly the beam charge.

Neutrons were selected in coincidence with the charge ''islands'' seen in the scatter plots of the raw analog-to-digital converter (ADC) response for the two charge measuring detectors BV and SSD. A typical scatter plot obtained using the interaction trigger, is shown in Fig. 1 for $^{40}$Ca projectiles with 565*A* MeV. The corresponding charge-

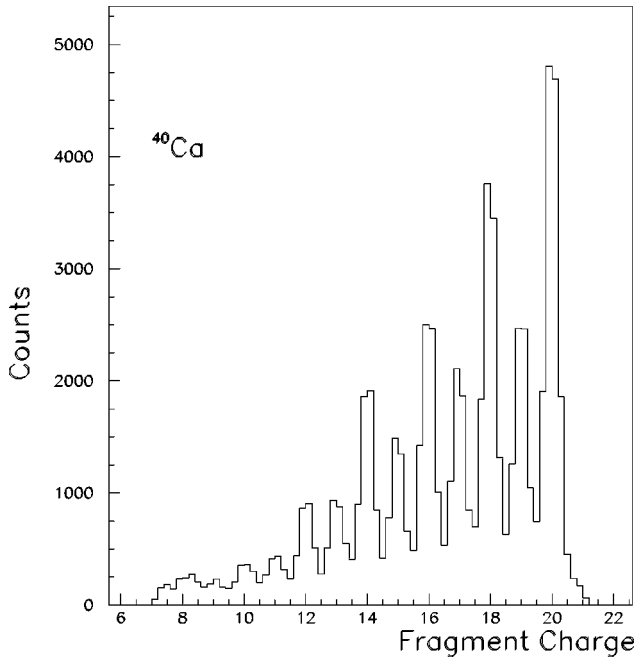


FIG. 2. A charge histogram for $^{40}$Ca at 565$A$ MeV, with the $Z$ scale properly calibrated [13].

spectrum, with the same trigger, after a proper charge calibration [13,15], is shown in Fig. 2.

### III. RESULTS

The neutron cross sections are reported in Table I. It is worthwhile to note that the cross section for $Z=20$ is a measure of the neutron stripping cross section in the considered reaction. In our case the number reported in Table I is the sum of the one- and two-neutron stripping contribution corresponding to the production of $A=39$ and $A=38$ fragments, respectively. At 565$A$ MeV we have detected neutrons in coincidence with fragment charges in the range $20 \leqslant Z \leqslant 10$, while at 357$A$ MeV the coincidence was taken with fragment charges in the range $18 \leqslant Z \leqslant 12$, due to lower statistics.

For $Z \leqslant 9$ (at 565$A$ MeV) or $Z \leqslant 11$ (at 357$A$ MeV) it was impossible to identify the fragment charge [15], as seen in Fig. 2 and, consequently, the neutron cross section in coincidence with these fragments. Those events, however, do contribute to the total inclusive neutron cross section [23].

TABLE I. Neutron cross sections (in coincidence with fragments with charge $Z$) for the $^{40}$Ca + H reaction at $E_{\rm lab}=565A$ and 357$A$ MeV.

| $Z$ | $\sigma_{n,565A\ \rm MeV}$ [mb] | $\delta\sigma$ [mb] | $\sigma_{n,357A\ \rm MeV}$ [mb] | $\delta\sigma$ [mb] |
|---|---|---|---|---|
| 20 | 20.0 | 10.0 | | |
| 19 | 11.0 | 7.0 | | |
| 18 | 28.0 | 6.0 | 13.0 | 4.0 |
| 17 | 18.0 | 5.0 | 8.0 | 3.0 |
| 16 | 35.0 | 6.0 | 12.0 | 4.0 |
| 15 | 20.0 | 4.0 | 17.0 | 11.0 |
| 14 | 30.0 | 5.0 | 15.0 | 6.0 |
| 13 | 18.0 | 4.0 | 6.0 | 2.0 |
| 12 | 21.0 | 5.0 | 6.0 | 3.0 |
| 11 | 8.0 | 3.0 | | |
| 10 | 6.0 | 3.0 | | |

The measured neutron cross sections are reported in the upper panels of Fig. 3 as a function of $Z$ for the two beam energies. In the lower panels of Fig. 3 we report the corresponding elemental production cross sections for the same reaction and energies [13,15]. Also reported in each panel of Fig. 3 are the corresponding theoretical cross sections, calculated in the frame of the Boltzmann-Nordheim-Vlasov approach (BNV) [5,23,25]. A soft equation of state has been used with compressibility $K=200$ MeV with a Skyrme type density dependent mean field. The production of neutrons, in coincidence with fragments with charge $Z$, is taken into account, in the calculations, as a second step by means of a phase-space coalescence calculation [25]. All calculations reported in this paper use a coalescence radius $D=3.5$ fm and $D=4.5$ fm for neutron and fragment production, respectively. Additional details of the calculations can be found in Ref. [23]. The model shows only a qualitative agreement with the absolute cross section data. Due to the fact that the neutrons have been selected in coincidence with the charged fragments emitted in the collision, the neutron cross sections exhibit, as expected, the same trend as the elemental cross sections [13], that is, a strong odd-even staggering attributed to the internal nuclear structure of the emitted fragments.

The experimental neutron production appears to be too small with respect to the number of free neutrons allowed by the size of the remnant fragment detected in coincidence. We have inferred the mean neutron multiplicity $M_n$ vs the remnant charge through the ratios between neutron and elemental cross sections $M_n=\sigma_n/\sigma_{\rm frag}$, at the two beam energies. In Fig. 4 we report $M_n$ vs $Z_f.\sigma_{\rm frag}$ has been obtained summing up all isotopic cross sections of Table I of Ref. [15], but excluding, for $Z=17$, 18, and 19, the case in which a fragment with $N=20$ has been produced.

The mean neutron multiplicity shows an increasing trend as $Z$ decreases. Lower multiplicities are found at the lower energy. However, as it is possible to infere from the data plotted in Fig. 4, the neutron multiplicity is always much smaller than the ''missing neutrons,'' defined as the number of neutrons necessary to form a $^{40}$Ca from the remnant. As we are going to show, this ''neutron defect'' can be explained only by making the hypothesis that a preequilibrium emission of prompt neutrons takes places in superposition to a ''slower'' deexcitation of the equilibrated remnant by emission of nucleons and fragments.

We cannot explain this observed ''neutron defect'' as due to clustering of neutrons in light fragments, particularly for the ones detected in coincidence with high-$Z$ fragments, that correspond to peripheral collision in which there are very few available nucleons, with unfavorable phase space conditions, to allow the necessary rate of light fragment emission. On the other hand, due to reverse kinematics, we expect most of the neutrons emitted by the remnant, which travels with a rapidity close to the beam rapidity, to enter the geometrical acceptance of MUFFINS. In fact, for a single source a simple maxwellian extrapolation of the neutron $p_t$ distribution given in Ref. [23] would predict that about 90% of the produced neutrons fall within the acceptance of MUFFINS. As a matter of fact the experimental $p_t$ slope corresponds to a temperature of 1 MeV [23], while it would be necessary at

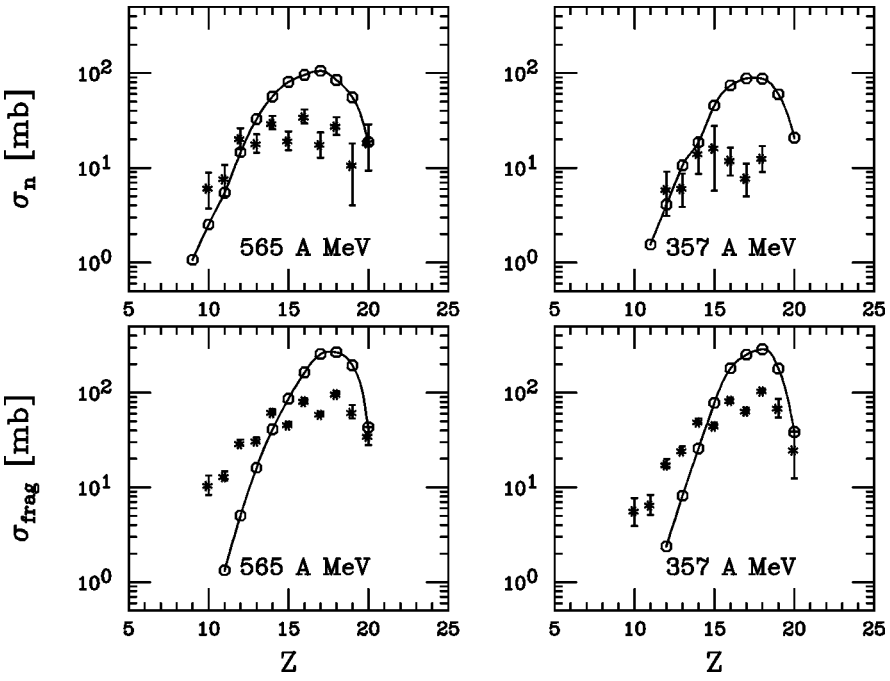


FIG. 3. Upper left panel: Measured neutron cross sections $\sigma_n$ (asterisks) for the $^{40}$Ca+H reaction at $E_{lab}=565A$ MeV, in coincidence with charged fragments, compared with the BNV +phase space coalescence model (circles joined by a solid line). Upper right panel: same for $E_{lab}=357A$ MeV. Lower panels: Elemental production cross sections $\sigma_{frag}$ (asterisks) for the same reaction and energies in comparison with calculations (circles joined by the solid line). Points at $Z=20$ are taken from Ref. [15].

least an order of magnitude greater temperature to explain the neutron defect.

A reasonable way to explain the observed neutron defect seems to be the existence of a double reaction mechanism, in which one mechanism is mainly responsible for the low energy neutrons, kinematically restricted in a small forward cone around 0°, while the other is able to produce energetic neutrons in a much wider angular range. So, as suggested also by other recent studies of reverse kinematics nuclear collisions [11], we interpret our data as the result of a two-step reaction: the ''neutron defect'' is caused by those neutrons emitted in a preequilibrium stage. Since the system is not yet thermalized and so the energy is not shared between a large number of degrees of freedom they can take a larger fraction of the transverse momentum and escape out of the MUFFINS angular coverage, effectively reducing the neutron multiplicity. Around 0° we detect on the contrary mainly neutrons emitted by the excited remnant, at low energy in the source frame, which show indeed the rapidly decreasing $p_t$ distribution already discussed.

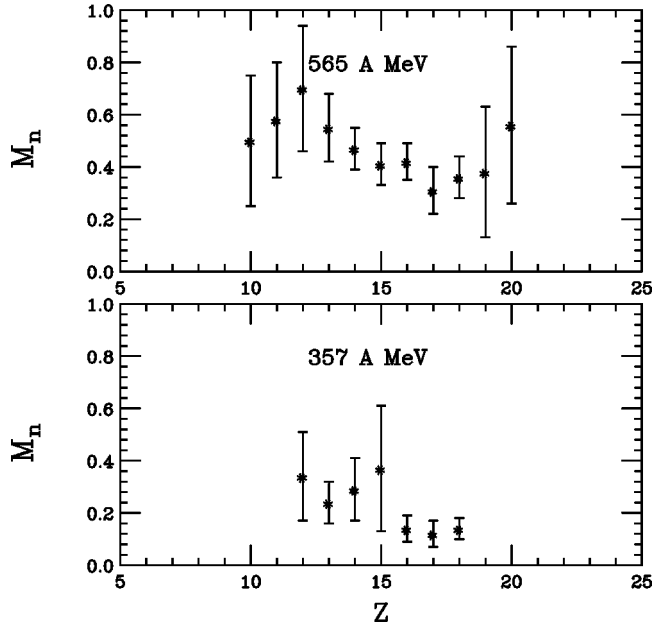


FIG. 4. (a) Mean neutron multiplicity versus Z for the $^{40}$Ca +H reaction at $E_{lab}=565A$ MeV. (b) The same at 357$A$ MeV.

Our interpretation is also supported by the neutron angular distribution reported in Fig. 2 of Ref. [23]: there we find a flatter distribution than the one predicted both by BNV calculation and by a thermal model (in the latter case, we have done simulations for temperatures ranging from $T=1-10$ MeV). This indicates that we have an unexpected neutron production at large angles, escaping from the angular acceptance of MUFFINS, which can be associated with the ''prompt'' emission step.

Furthermore, the inclusive neutron rapidity distribution presented an asymmetric tail at low rapidities, as shown in Fig. 4(a) of Ref. [23], which already in that paper was attributed to a possible first-step emission. As a matter of fact, due to the specific features of our reaction (collision between ''large'' and ''small'' nuclei) these neutrons could be produced, very likely, locally along the proton target path in the much larger projectile. They should undergo a more violent interaction with the proton target and, therefore, acquire a large transverse momentum. Some of those should be, therefore, detected by MUFFINS in the low rapidity region. On the contrary, for events close to beam rapidity ($y/y_{beam}\geqslant 0.85$), the $T=1$ MeV value extracted from the $p_t$ distribution [23] indicated that neutrons should come from a remnant which carried small excitation energy.

The same type of evidence is found in neutron rapidity distributions taken in coincidence with fragments, as, for example, the ones in coincidence with $Z=18$ and $Z=12$ at 565$A$ MeV reported in Fig. 5. They show a peak around beam rapidity while a tail at lower rapidity is still present, even if affected by large error bars.

In conclusion, we interpret the fact that the neutron multiplicity in Fig. 4 is smaller than expected with the emission

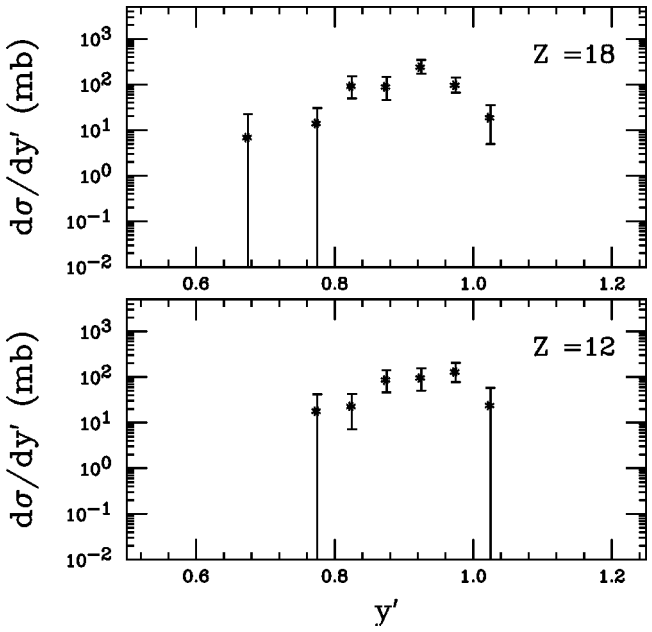


FIG. 5. Neutron rapidity distribution in coincidence with $Z=12$ and $Z=18$ fragments ($y'=y/y_{\mathrm{beam}}$).

of prompt neutrons that are for the most part not seen in our detector due to its relatively small angular coverage. The energy dependence of the neutron production is better investigated looking at the ratios in Fig. 6. In this figure we report the ratio $R_n=\sigma_n(E=565A\ \mathrm{MeV})/\sigma_n(E=357A\ \mathrm{MeV})$ in the upper panel and $R_{\mathrm{frag}}=\sigma_{\mathrm{frag}}(E=565A\ \mathrm{MeV})/\sigma_{\mathrm{frag}}(E=357A\ \mathrm{MeV})$, for the fragments, in the lower panel.

In the lower part of Fig. 6 the ratio $R_{\mathrm{frag}}$ shows that almost no energy dependence is observed in the elemental cross sections for fragment charge from the beam charge down to $Z\simeq 15$. This is in a quite good agreement with BNV calculations, which reproduce relative cross sections better than absolute ones. The situation is less clear for the neutron data due to larger error bars. Anyhow, the general trend observed in the data, upper part of Fig. 6, seems to be consistent with the theoretical predictions and with the fragment production data if one considers that at the lower incident energy due the weaker focussing in the forward direction more neutrons are lost outside the angular range covered by MUFFINS ($0°-3.2°$). This is suggested, on the other hand, by the lowest values of multiplicity at $E=357A$ MeV.

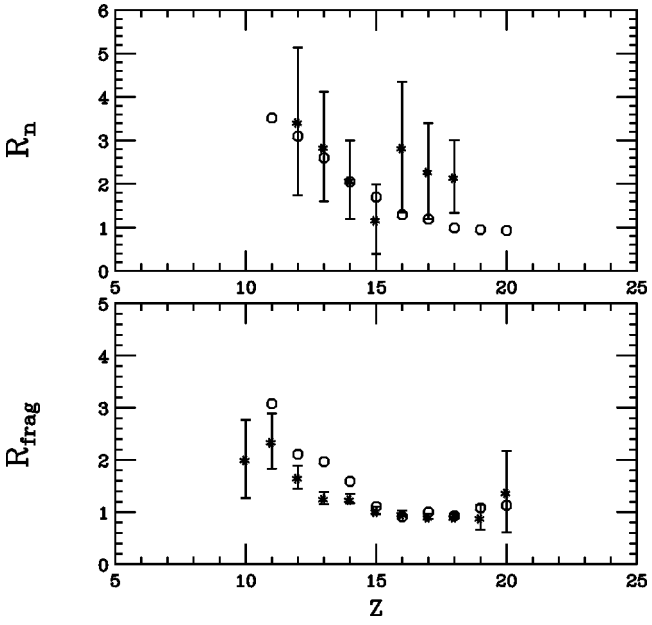


FIG. 6. Upper panel: Ratio $R_n=\sigma_n(E=565A\ \mathrm{MeV})/\sigma_n(E=357A\ \mathrm{MeV})$ (asterisks) versus $Z$ measured in $^{40}$Ca + H reaction in comparison with calculations (circles). Lower panel: Ratio $R_{\mathrm{frag}}=\sigma_{\mathrm{frag}}(E=565A\ \mathrm{MeV})/\sigma_{\mathrm{frag}}(E=357A\ \mathrm{MeV})$ (asterisks) versus $Z$ measured in the same reaction in comparison with calculations (circles).

In addition, the trend observed for both ratios of Fig. 6 could be traced back to the centrality of the collisions: smaller fragments are produced in central collisions while peripheral collisions are responsible for the production of fragments with $Z\geqslant 15$. From this point of view, triggering on a given $Z\leqslant 15$ fragment is roughly equivalent to selecting central collisions.

The more destructive central collisions bring in a larger energy dependence. This is not very surprising, since one would expect the number of nucleon-nucleon collisions, and therefore the maximum possible energy transfer, to be smaller at large impact parameters (peripheral collisions) as suggested, on the other hand, by our BNV calculations.

## IV. CONCLUSIONS

In conclusion, we have presented new neutron production data in coincidence with fragments emitted in the reaction $^{40}$Ca + H and suggested an interpretation for the inferred mean multiplicity and energy dependence of the neutron cross sections. Our data show evidence of a two-step reaction mechanism already discussed in connection with very asymmetric nuclear collisions [8,9,11]. We interpret the observed neutron defect as due to a preequilibrium emission of energetic neutrons that escape from the angular coverage of our detector. The small value obtained for the inverse slope in the transverse momentum distribution of the neutrons travelling with the beam rapidity suggests that very little excitation energy is deposited into the system. Those neutrons are, therefore, emitted by the remnant in the second step of the reaction. We have established that the overall experimental findings of the elemental production are in agreement with the picture that emerges from BNV + phase space coalescence calculations especially for relative cross sections.

More data and further theoretical investigations are necessary for a better understanding of the neutron production. Both of them should be available in the near future.

## ACKNOWLEDGMENTS

The U.S. members of the TRANSPORT Collaboration acknowledge support for this work by NASA under Grants No. NAGW-1526, NGR 05-003-513, NAGW-2004, NAGW-3022, and L14230C and by the U.S. DOE under Grant No. DE-FG05-ER 40147.

[1] H. Gutbrod, A. M. Poskanzer, and H. G. Ritter, Rep. Prog. Phys. **52**, 1267 (1989).
[2] A. Insolia, U. Lombardo, N. Sandulescu, and A. Bonasera, Phys. Lett. B **334**, 12 (1994).
[3] G. F. Bertsch and S. Das Gupta, Phys. Rep. **160**, 189 (1988).
[4] W. Cassing, V. Metag, U. Mosel, and K. Niita, Phys. Rep. **188**, 363 (1990).
[5] A. Bonasera, F. Gulminelli, and J. Molitoris, Phys. Rep. **243**, 1 (1994).
[6] J. P. Wefel, in *Genesis and Propagation of Cosmic Ray*, edited by M. M. Shapiro and J.P. Wefel (Reidel, Dordrecht, 1988).
[7] T. G. Guzik *et al.*, *Proceedings of the 25th International Cosmic Ray Conference, Durban*, South Africa, 1997, edited by M. S. Potgieter, B. C. Raubenheimer, and D. J. van der Walt, Westprint (Potchefstroom, 1997), Vol. 4, p. 317.
[8] M. Mahi *et al.*, Phys. Rev. Lett. **60**, 1936 (1988).
[9] T. Porile *et al.*, Phys. Rev. C **39**, 1914 (1989).
[10] J. Pochodzalla, Prog. Part. Nucl. Phys. **39**, 443 (1997).
[11] J. A. Hauger *et al.*, EOS Collaboration, Phys. Rev. C **57**, 764 (1998).
[12] C.-X. Chen *et al.*, TRANSPORT Collaboration, Phys. Rev. C **49**, 3200 (1994).
[13] C.N. Knott *et al.*, TRANSPORT Collaboration, Phys. Rev. C **53**, 347 (1996).
[14] S. Albergo *et al.*, TRANSPORT Collaboration, Radiat. Meas. **27**, 549 (1997).
[15] C.-X. Chen *et al.*, TRANSPORT Collaboration, Phys. Rev. C **56**, 1536 (1997).
[16] R. Madey, J. Varga, A. R. Baldwin, B. D. Anderson, R. A. Cecil, G. Fai, P. C. Tandy, J. W. Watson, and G. D. Westfall, Phys. Rev. Lett. **55**, 1453 (1985).
[17] R. Madey *et al.*, Phys. Rev. C **42**, 1068 (1990).
[18] M. Elasaar *et al.*, Phys. Rev. C **49**, R10 (1994).
[19] D. Lambrecht *et al.*, Z. Phys. A **350**, 115 (1994).
[20] Y. Leifels *et al.*, Phys. Rev. Lett. **71**, 963 (1993).
[21] S. Albergo, S. Costa, M. Mazzeo, D. Nicotra, G. Poli, R. Potenza, C. Tuvé, H. J. Crawford, and I. Flores, Nucl. Instrum. Methods Phys. Res. A **311**, 280 (1992).
[22] S. Albergo *et al.*, Nucl. Instrum. Methods Phys. Res. A **362**, 423 (1995).
[23] C. Tuvé *et al.*, TRANSPORT Collaboration, Phys. Rev. C **56**, 1057 (1997).
[24] W.M. Zhang *et al.*, Phys. Rev. C **52**, 2643 (1995).
[25] A. Bonasera, M. Colonna, M. Di Toro, F. Gulminelli, and H.H. Wolter, Phys. Lett. B **244**, 169 (1990).